Numerical Investigation of Tension Behavior of Reinforced Concrete Members Strengthened with FRP Sheets

Khalid Farah*, Yasuhiko Sato**

* PhD Candidate, Division of Built Environment, Hokkaido University, Sapporo, 060-8628
** Assoc. Professor, Division of Built Environment, Hokkaido University, Sapporo, 060-8628

This paper presents numerical simulation of the tension behaviour of reinforced concrete (RC) members strengthened with externally bonded carbon fiber sheets (CFS) by using two dimensional (2D) rigid body spring model (RBSM). A non-linear RC model strengthened with CFS with bond-slip relations to model the concrete, steel reinforcement interface and concrete, externally bonded CFS interface, and simple models for bond deterioration due to cracking was embedded in the RBSM code that was developed by the authors. Comparison between the RBSM prediction and experimental results shows good agreement. The CFS has shown significant change in the bond stress and average stress of steel reinforcing bar and concrete. In addition the CFS has reduced the crack spacing and gave good crack width control.
Keywords: Reinforced concrete, Numerical, CFS, RBSM

1. INTRODUCTION

Extending the service life of the existing RC structures is one of the major tasks of the civil engineering. Strengthening or retrofitting is one of the remedial actions to perform this task. Strengthening or retrofitting the RC members by using fiber reinforced polymer (FRP) sheets as external bonding has become very popular technique nowadays, due to the superior characteristics of FRP sheet such as; high strength, high stiffness-to-weight ratio, high corrosion resistance, good fatigue strength, potential for decreasing the instillation costs due to lower weight in comparison to steel, and ease of application in the site.

Bonding between FRP sheet and concrete is very important to ensure composite action between concrete and FRP sheet. Loss of bonding would cause undesirable premature failure prior to the theoretical or predicted ultimate load. Although there are many studies on bond behavior of FRP sheets (Japan Concrete Institute[4], Japan society of Civil Engineers[5], Sato et al.[6] and Ueda et al.[7]), the tension behavior of reinforced concrete member strengthened with FRP Sheets is not well clarified yet. In addition there is no numerical models available to simulate this behavior. This study was conducted to provide numerical model to simulate the pure tension behavior of concrete element with internal reinforcement and external FRP sheets. This numerical simulation is need to clarify the effect of FRP sheets on the relationship of average bond stress-average strain of steel reinforcement and FRP sheet, average strain-average stress for Steel reinforcement and concrete and average crack spacing .

2. EXPERIMENTAL OVERVIEW

In this study part of the experiments that had been done by Ueda et al.[7] will be use as experimental evidence. Specimens were concrete prisms with cross section of 150×150 mm with a deformed bar embedded at their center of the cross section and carbon fiber sheets (CFS) externally bonded to their two side surfaces, as shown in Fig.1. The experimental parameters were the steel reinforcement ratio (ρ_s) and FRP sheet ratio (ρ_{CFS}) as shown in Table 1. The width of the CFS was narrower than prism width where the prism width was 150 mm and the CFS width was 120 mm. Strain gauge were mounted on the steel bar at 40 mm spacing and on the top layer of CFS at 20 mm spacing in the test zone of 1200 mm. Contact chips were mounted on the concrete surface at 60 mm spacing to measure the crack widths. Both ends of the prisms were reinforced by steel plate and lateral reinforcement. All the specimens were pulled statically through a deformed bar embedded in the concrete prism by a hydraulic jack. Strains of the reinforcing bar and CFS as well as concrete crack widths were measured. The local bond stresses that will be used later were calculated from the measured strains, by using equation 1.

$$\tau = \frac{AE \ \Delta \varepsilon}{A_{bo} \ \Delta x} \quad (1)$$

where A and E are cross-sectional area (mm^2) and Young's modulus (MPa) of the steel bar reinforcement/CFS; A_{bo} is bonding area per unit length (mm); $\triangle\varepsilon$ is the difference in the strain of the steel bar reinforcement/CFS; and $\triangle$x is the difference in the location (mm). The concrete compressive strength was 30 MPa for all specimens. The material properties of the deformed bars and CFS are shown in Tables 2 and 3, respectively.

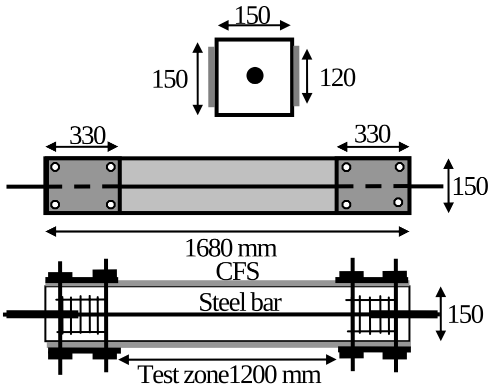

Fig. 1 Specimen layout

Table 1 Details of Specimens

Specimen	Type of reinforcement bar	Cover (mm)	AC (mm*mm)	ρ_s	ρ_{CFS}
S-3-0	D19	65.5	150*150	1.27	0
S-3-1	D19	65.5	150*150	1.27	0.12
S-3-2	D19	65.5	150*150	1.27	0.23

Table 2 Material Properties of Reinforcement Bars

Steel bar	Diameter (mm)	E_s (GPa)	ε_y (%)
D19	19.1	170	0.23

Note: E_s=Young's modulus; ε_y=Yielding strain

Table 3 Materials Properties of Carbon Fiber Sheet

t (mm)	ρ (g/m^2)	F_t (MPa)	E_{CFS} (GPa)	ε_u (%)
0.11	200	3479	230	1.5

Note: t=Thickness; ρ=Fiber Density; F_t=Tensile Strength; E_{CFS}= Young's modulus; ε_u=Fracture strain

3. NUMERICAL APPROACH

Both experimental and numerical investigations of materials and structures should be incorporated into the development of reasonable design code. Recently the numerical methods that had been applied to simulate the structural behavior of reinforced concrete members and structures under various types of loading or materials types had become more effective due to the advance in computing technology. There are several numerical approaches to simulate the behavior of reinforced concrete members.

The finite element method (FEM) had been applied to provide the over-all performance of reinforced concrete structure. FEM provides reasonable prediction for loading capacity and formation of cracks but in the same time it is hard to get realistic fracture condition such as crack pattern and so on.

The discrete methods have the ability to model the materials discontinuity and the brittle failure mode plus the localization process which accompany the fracture of brittle material.

The advance design processes require direct understanding of damage evaluation and failure mode plus the loading capacity. So that the numerical model that can predict the fracture condition, crack formation and propagation plus the overall performance is highly required.

The rigid body spring model which was first developed by Kawai[1)] is one of the discrete methods. RBSM will be used in this study as numerical approach instead of the common FEM; because of its simplicity in modeling the different materials discontinuity (concrete, steel reinforcement and CFS) and it is ability to provide reasonable prediction for loading capacity, crack initiation and propagation and overall performance [2]. RBSM has the ability to describe the localization process which accompanies the fracture in brittle-matrix composite materials like the failure of CFS or CFS-concrete interface (debonding). The proposed numerical model was embedded in the RBSM code that was developed by the authors to simulate the experimentally observed phenomena.

3.1 Rigid Body Spring Model

The rigid body spring model (RBSM) represents the continuum material as an assemblage of rigid particle elements interconnected along their boundaries through flexible interface. The interface may be viewed as zero-size springs whose initial properties can be set to approximate the overall elastic properties of the continuum. The response of the spring model provides comprehension of the interaction between particles instead of the internal behavior of each particle based on a continuum mechanics.

Each rigid particle has three degree of freedom are defined at the arbitrary point within the particle; two translations and one rotational degree of freedom. The flexible interface between particles (interparticle boundaries) consists of three springs in the normal, tangential and rotations as shown in Fig. 2. Since concrete cracks initiate and propagate along interparticle boundaries, the fracture directions and crack pattern is strongly affected by the mesh design. So that the material will be partition into an assemblage to rigid particles by using random geometry using Voronoi diagrams to reduce the mesh bias on potential crack directions (Bolander and Saito[3]).

3.2 Concrete Models

Fracture initiation and propagation are modeled by successfully introducing fracture criterion of concrete material into spring properties. Fracture criterion in RBSM is not based on a tensorial measure of stresses, but utilizes the average stresses acting normal and tangential to the particle interface. The criterion is rather simply constructed. That is, uni-axial stress-strain relationships can be introduced into the individual springs.

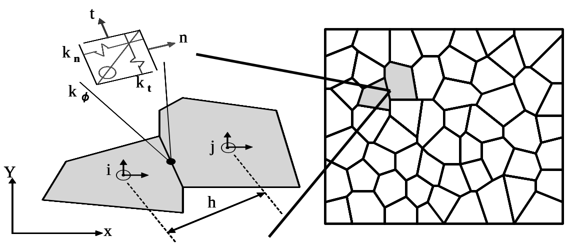

Fig. 2 Rigid Body Spring Model

In this study the concrete in compression shows nonlinear behavior up to the compressive strength then after the peak the linear softening branch take place till failure. Fig. 3 shows the relationship that modeled by equation (2).

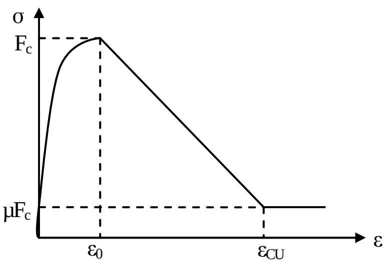

Fig. 3 Compression model of concrete

$$\sigma=\begin{cases} E\varepsilon-\dfrac{E}{2\varepsilon_0}\varepsilon^2 & for \quad \varepsilon\le\varepsilon_0 \\ F_c-\left(\dfrac{F_c-\mu F_c}{\varepsilon_{CU}-\varepsilon_0}\right)(\varepsilon-\varepsilon_0) & for \quad \varepsilon_0<\varepsilon\le\varepsilon_{CU} \\ \mu F_c & for \quad \varepsilon>\varepsilon_{CU} \end{cases} \qquad (2)$$

where; E=modulus of elasticity (MPa) , F_c=compressive strength (MPa), ε= compression strain, $\varepsilon_0=2F_c/E$, $\varepsilon_{CU}=4\varepsilon_0$, μ=0.2.

Concrete in tension behaves linearly elastic up to tensile strength then the stress-strain relationship exhibits strain softening till failure. The softening part depends on the crack width (Hordijk[8]) as shown in equation (3)

$$\frac{\sigma}{F_t}=\left\{1+\left(C_1\frac{W}{W_C}\right)^3\right\}\exp\left(-C_2\frac{W}{W_C}\right)-\frac{W}{W_C}(1+C_1^3)\exp(-C_2) \qquad (3)$$

$$W_C=5.14\frac{G_F}{F_t}$$

$$G_F=10(D_{max})^{1/3}F_c^{1/3}$$

where: W=crack width (10^{-6} m), σ =tensile stress (MPa), C_1=3, C_2=6.93, W_C= critical crack width where no stress can be transferred (10^{-6} m), G_F= fracture energy (N/mm), D_{max}= maximum size of aggregate (mm).

3.3 Reinforcement Model

Each reinforcement bar is modeled by using one-dimensional beam elements with axial, shear and flexural rigidities. Two translational and one rotational degree of freedom are defined at each beam element end as shown in Fig. 4 (Saito and Bolander[9]). The stress-strain relationship of reinforcement was used as tri-linear model as in equation (4).

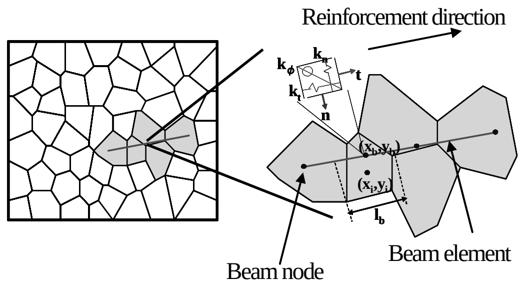

Fig. 4 Continuous reinforcement with zero-size linkage element

$$\sigma=\begin{cases} E_s\times\varepsilon & \varepsilon<\varepsilon_y \\ E_s\times\varepsilon_y & \varepsilon_y\le\varepsilon<\varepsilon_h \\ E_s\times\varepsilon_y+E_h\times(\varepsilon-\varepsilon_y) & \varepsilon\ge\varepsilon_h \end{cases} \qquad (4)$$

where; E_s is the modulus of elasticity (MPa), ε is the steel strain, ε_y is the yielding strain, ε_h is the strain when hardening strain starts and E_h (MPa) is the stiffness when the strain hardening starts.

The reinforcement is connected to the concrete particle element through zero-size linkage elements to represent the bond slip property. One of the linkage nodes is attached to the reinforcement, while the motion of the other link node is rigidly constrained to the generalized displacement of the associated computational point as shown in Fig. 4.

The bond-slip interaction between concrete and reinforcing material strongly affects crack distributions and stress of steel reinforcement bar. The bond-slip will be represented by introducing the bond slip relation into the linkage element spring parallel to steel reinforcing bar. The bond slip model proposed by Shima et al.[10] and modeled by equation (5) will be used.

$$\frac{\tau}{F_c} = \frac{0.73\,(\ln(1+5s))^3}{1+\varepsilon \times 10^5} \qquad (5)$$
$$s = 1000 \;\; S / D$$

where: τ=bond stress (MPa), S=slip (mm), D=bar diameter (mm), ε=steel strain

3.4 FRP sheet Model

For FRP sheet the same beam element that had been used for steel reinforcement will be used. The stress strain relation ship had been used as linear relation up to failure. The bond stress- slip-strain model proposed by Sato et al.[6] had been introduced into the linkage spring parallel to the FRP sheet to simulate the bond slip interaction between FRP sheet and concrete. The model shows non-linear parabolic curve for pre peak bond stress then after the peak the non linear softening branch takes place (equation (6)).

For pre-peak regime

$$\tau = \frac{148\,S}{1+1000\,\varepsilon} F_c^{0.2} \qquad (6a)$$

For post-peak regime

$$\begin{aligned}
&\tau = \tau_{\max}.EXP(-10(S-S_0)) \\
&\tau_{\max} = 9.1F_c^{0.2}.tE_{CFS} \times 10^{-5} \qquad \le 3.49\,F_c^{0.2} \\
&tE_{CFS} \le 38.4GPa \\
&S_0 = 0.8\times10^{-12}(tE_{CFS})^{2.4} F_c^{0.2} + 0.021 \qquad (6b) \\
&tE_{CFS} > 38.4GPa \\
&S_0 = \frac{3100}{tE_{CFS}} F_c^{0.2} + 0.034
\end{aligned}$$

where; τ = local bond stress (MPa), S=local slip (mm), F_c= concrete compressive strength (MPa), ε= CFS strain, E_{CFS}= CFS elastic modulus (MPa) and t= CFS thickness (mm).

3.5 Bond Deterioration Model for Steel Reinforcement

Splitting conical cracks appear, when reinforcing bar is tensioned against concrete, because the ribs of the reinforcing bar press against concrete causing conical diagonal compressive struts (Goto[11]). In direction perpendicular to these compressive struts Tensile stresses are generated causing these splitting conical cracks. In the vicinity of crack planes, these compressive struts have no concrete to support because of the penetration of conical cracks reaching to the crack planes. So that, concrete spalling takes place causing bond deterioration as shown in Fig. 5 (Qureshi and Maekawa[12]). Shima's model can not be applied to that bond deterioration zone where the near crack surface effect is the predominant (Okamura and Maekawa[13]). The modeling of bond in the cracks locations is important for the post yield behavior because the localization of plastic yielding is initiated from the bond deterioration zone. Qureshi and Maekawa[12] in the RC joint model, proposed bond deterioration model as shown in Fig. 5. where the bond stress is decreasing in linear fashion till zero value in distance equal 5D from the crack surface, where D is the bar diameter, and the bond stress drops suddenly to zero at a distance equal 2.5D from the crack surface due to splitting and crushing of concrete around the bar beside the crack surface.

Salem and Maekawa[14] had modified Qureshi and Maekawa[12] bond deterioration model for small crack spacing where, they proposed that bond deterioration zone is not fixed length (5D) but it depends on the crack spacing. The bond deterioration zone varied from 5D for crack spacing equal 10D to zero for crack spacing equal 5D or less as shown in Fig. 6.

In this study simple bond deterioration model based on the previous models was proposed as shown in Fig. 7, the bond stress decrease linearly from maximum bond stress to zero in bond deterioration zone equal (2D). This simplified model had proposed to cover both control specimen and strengthened specimens because the crack spacing is changed from (15D) in control specimen to (5D) in strengthened specimen.

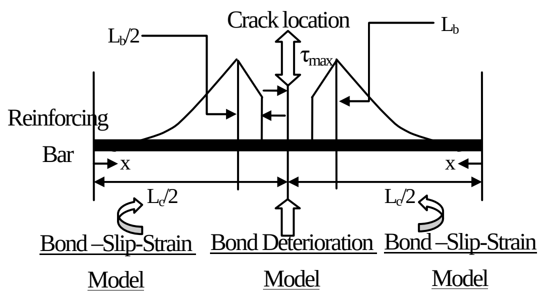

Fig. 5 Bond deterioration close to cracks (Qureshi and Maekwa[12])

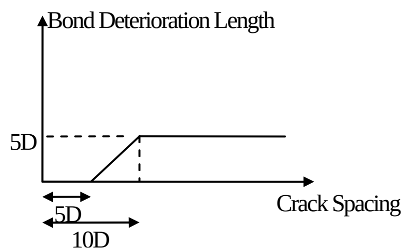

Fig. 6 Modification of bond deterioration model for small crack spacing (Salem and Maekawa[14])

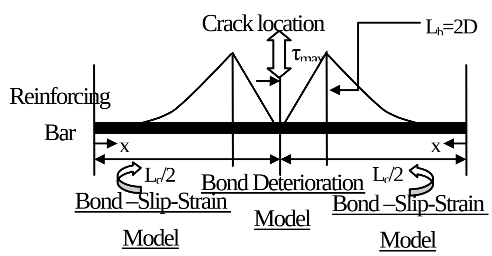

Fig. 7 Proposed simplified bond deterioration model

3.6 Bond Deterioration Model for FRP Sheet.

Although there are many studies on bond behavior of continuous fiber sheet, there are very few studies that focus on the deterioration of this bond and what the mechanisms of that deterioration.

Figure 8 indicates the variation of maximum bond stress with different locations (Sato et al[6]). The maximum bond stress decreases linearly till 50% from the maximum bond stress in distance equal 30 mm from the starting point of delamination and becomes constant beyond this point up to 80 mm from the maximum bond stress location then the bond stress can reach the maximum bond stress again (Sato et al[6]). It was assumed that the decrease in maximum bond stress is caused by the start of delamination (where the maximum bond stress corresponds to the point at which the delamination begins). So the reason for the decrease in maximum bond stress and variation of maximum bond stress with location can be explained as follow. The bonding layer of the concrete surface fracture at the point when the maximum bond stress is reached (delamination starts). This fracture induces mechanical damage in the bonding layer surrounding the fracture, because the fracture zone has a finite length. The bonding layer originally has the same strength as at the point of delamination starting when there is no damage how ever, once damage occurs; delamination can take place with less bond stress. However, as delamination and damage move further away from the delamination starting point the degree of damage is reduced until it finally reaches negligible level at a certain distance, this distance was observed to be 80 mm as in Sato et al[6].

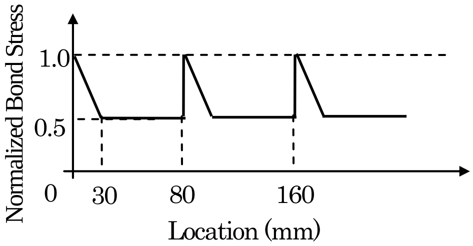

Fig. 8 Bond strength distribution (Sato et al.[6])

Ueda et al.[7] proposed other reasons for bond deterioration. The bond deterioration takes effect near the main cracks due to formation of diagonal cracks which induced by the CFS bond near the main cracks. Also, the bond deterioration takes effect when the reversed CFS slip appears near the main cracks due to the small crack spacing.

To simulate the bond deterioration due to cracking. Yamaguchi[15] proposed bond deterioration model based on Sato's bond model (Sato et al.[6]) as shown in Fig. 9. The maximum bond stress equal to zero at the crack surface then increasing linearly from zero to maximum bond stress in distance equal 60 mm from the crack location. Then the maximum bond stress decrease linearly from the maximum to 50% of the maximum bond stress at point with location equal 90.0 mm. The proposed bond deterioration is shown in Fig. 9. The maximum bond stress equal zero at crack location, then it increases linearly from zero to 70% from the maximum bond stress in distance equal 30 mm from the crack location. Beyond this point the maximum bond stress remain constant at 70% of the maximum bond stress.

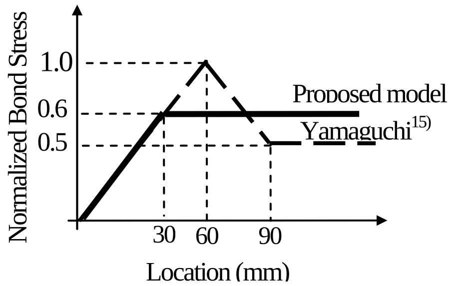

Fig. 9 Bond deterioration models in CFS

4. NUMERICAL RESULTS AND DISCUSSIONS

Comparison between the numerical and experimental results for strain distribution of the reinforcing steel bar and CFS in specimen S-3-0 and S-3-1 for different loads are shown in Fig. 10. There is very good agreement between the experimental and numerical results for the different loads which indicates the validity of the proposed models to simulate the member behavior in accepted manners. The agreement between the experimental and numerical strain values for both steel reinforcement/CFS especially near the crack locations implies the validity of the proposed bond deterioration model for steel reinforcement/CFS. In specimen S-3-1 with CFS, the crack spacing was smaller than in specimen S-3-0 without CFS. As result, the strain distribution in specimen S-3-1 is flatter than in specimen S-3-0, which means that the average bond stress is less.

Figure 11 shows the relationships between the average bond stress and the average strain of the steel bar reinforcement. For the experimental results, the average bond stress was calculated as the average of local bond stress in the test zone, while the average strain was calculated as the average of the local measured strain. For the numerical results the average bond stress was calculated as the average of the local bond stress of the bond springs for the steel/CFS elements which located in the test zone, the average strain was calculated as the average values of the strain of steel/CFS elements which located in the test zone. Fig. 11 shows clearly that the average bond stress in specimen S-3-0 without CFS is greater than those in specimens with CFS (specimens S-3-1 and S-3-2). Comparing to the steel strain the CFS strain in Fig. 10 (c) indicates greater localization at cracking. This means that the bond properties of the CFS are better than the bond properties of the steel reinforcement deformed bar.

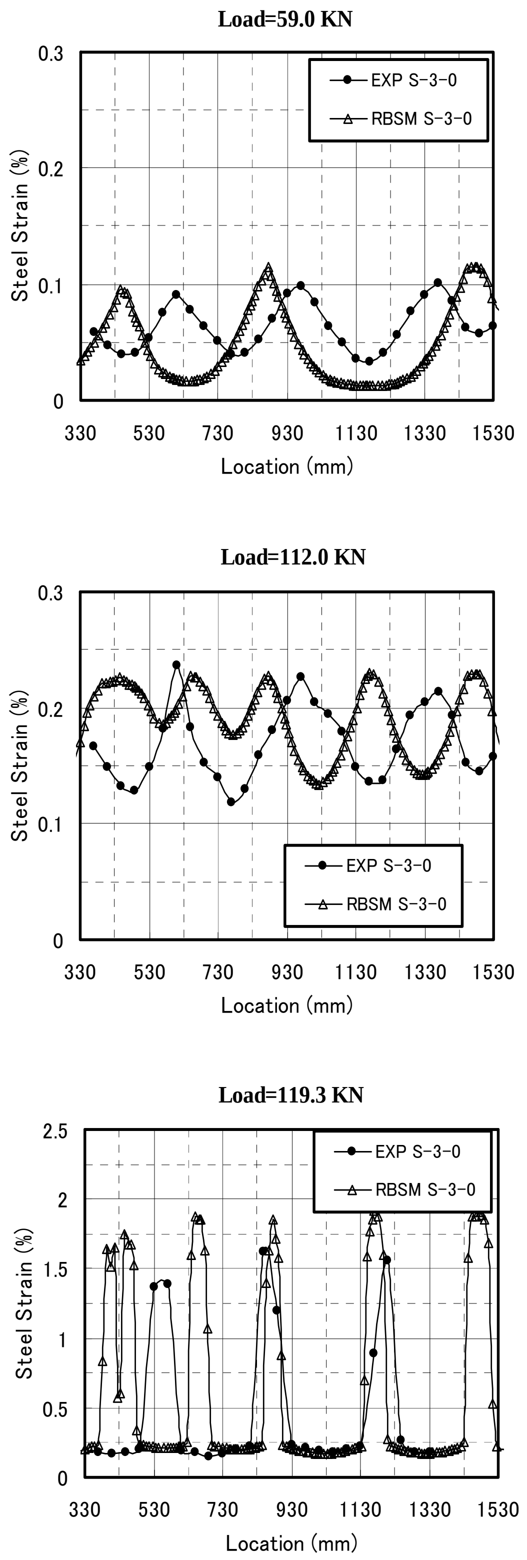

(a) Un-strengthened specimen (S-3-0)
Fig. 10 Strain distribution

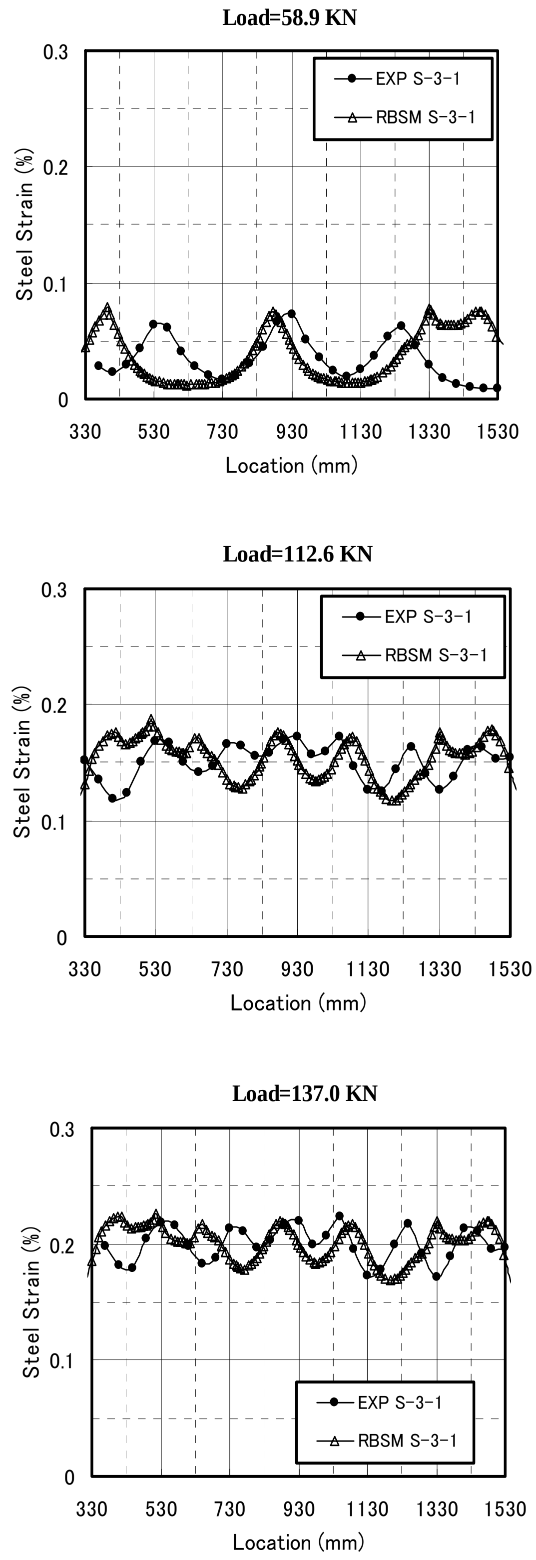

(b) Strengthened specimen (S-3-1)
Fig. 10 Strain distribution

Load=58.4 KN

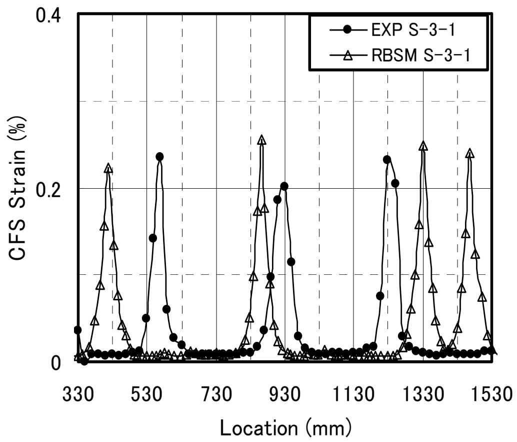

Load=112.6 KN

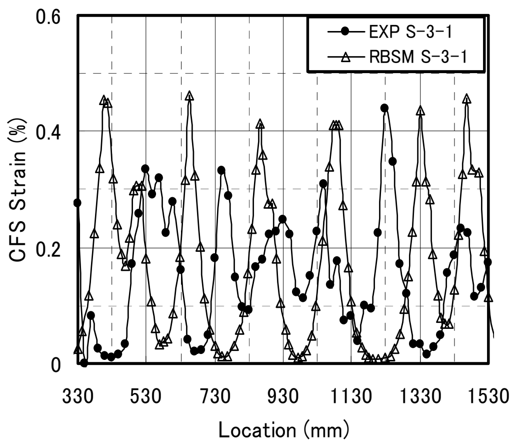

Load=155.4 KN

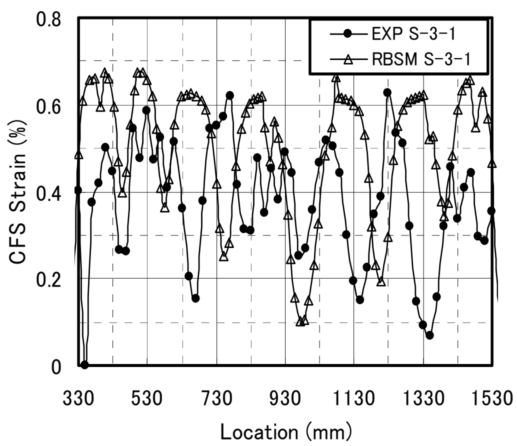

(c) Strengthened specimen (S-3-1)

Fig. 10 Strain distribution

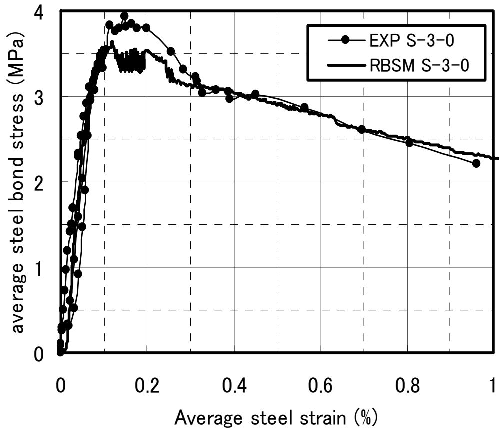

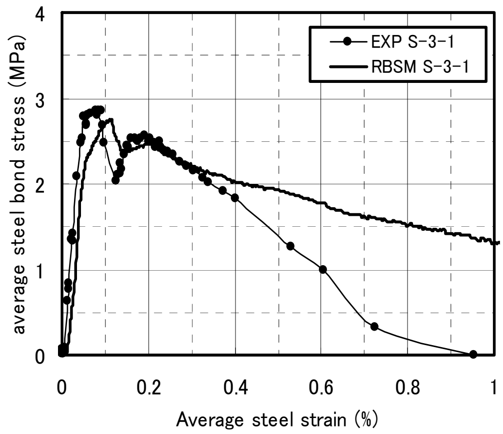

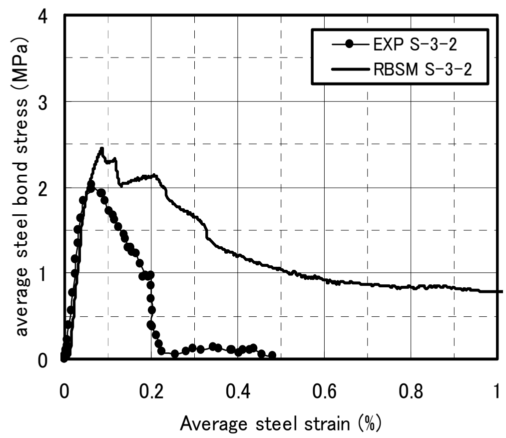

Fig. 11 Average bond stress-average strain in steel reinforcement

In Fig. 11 comparison between the experimental and numerical results for the relationships between the average bond stress and the average strain of the steel bar reinforcement for different specimens was presented. There were satisfied agreement between the experimental and numerical findings for un-strengthened specimen S-3-0 and strengthened specimens. For the post peak part of specimen S-3-2, there was not very good agreement between the experimental and numerical results.

The reason for this poor agreement is till under discussion and in the same time it is believed that the reason for this part is the scatter in the experimental results due to error in measuring the steel strain specially after peak where many cracks opens and crack width increases which leads to breakage of some strain gauges.

The relationship between the average bond stress and the average strain of CFS are given in Fig. 12. CFS with greater stiffness (or more layers) indicates greater average bond stress than CFS with a smaller stiffness. Peak average bond stress was observed experimentally after the delamination of CFS where the softening part starts to take place as shown in the numerical results. The satisfied agreements between the experimental and numerical findings prove the validity of the model and the bond deterioration model for CFS to simulate the bond deterioration near the cracks locations.

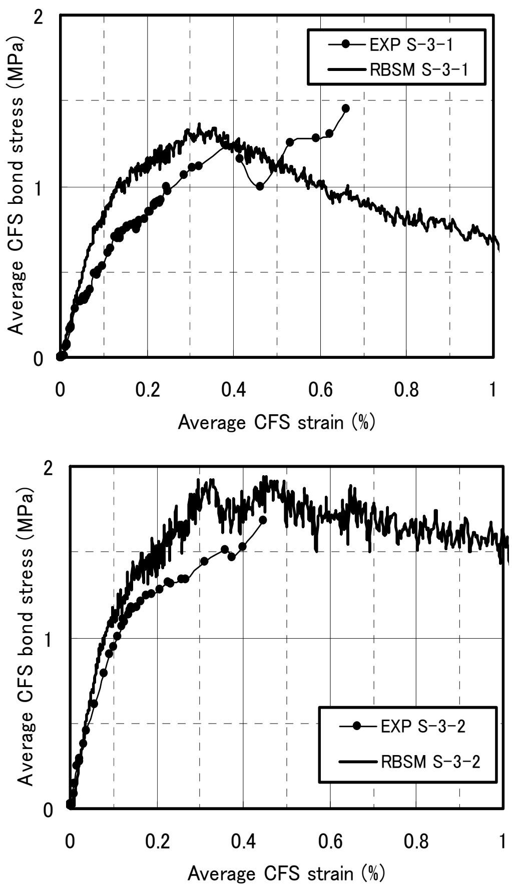

Fig. 12 average bond stress-average strain in CFS

The average stress- average strain relationship of the steel bar reinforcement in Fig. 13 is compared with the stress-strain relationship of the bare bar (not in concrete). The results show the capability of the proposed model to simulate the structural behavior in accepted way. The results indicate that the yielding stress is smaller than that of the bare bar due to the fact that the yielding takes place only at the crack intersection, and that the strains between cracks are still smaller than the yielding strain at that time. Figure 8 shows that the greater CFS ratio makes the relationship closer to the bare bar, this because a greater CFS ratio brings smaller crack spacing and then smaller bond stress between the steel bar and concrete.

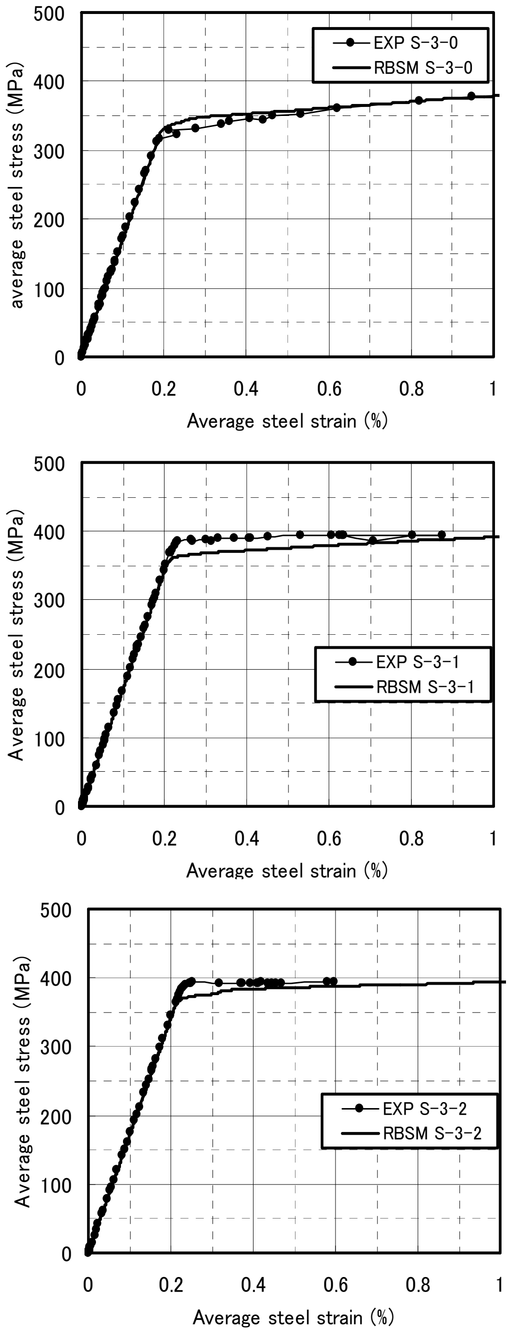

Fig. 13 average stress-average strain in steel reinforcement

Figure 14 shows the crack pattern for the different specimens in numerical and analysis. By comparing between the experimental and numerical analysis very good correlation can be found between crack spacing for the different specimens. The average crack spacing decrease significantly one the reinforced concrete member were strengthened with CFS, and decrease gradually as the CFS ratio increase as shown in Fig. 14

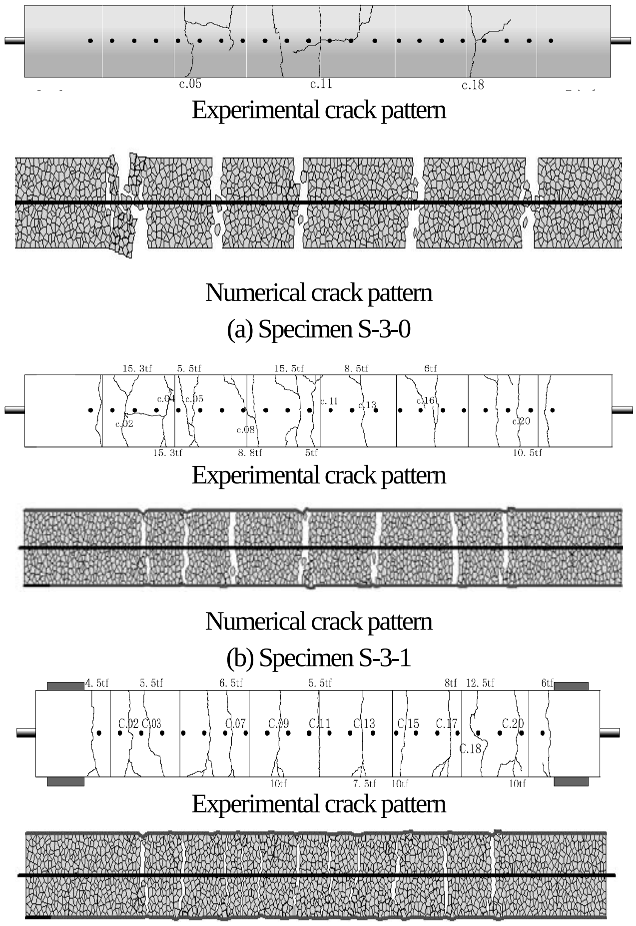

Experimental crack pattern

Numerical crack pattern

(a) Specimen S-3-0

Experimental crack pattern

Numerical crack pattern

(b) Specimen S-3-1

Experimental crack pattern

Numerical crack pattern

(c) Specimen S-3-2

Fig. 14 Crack patterns for numerical and experimental observation

5. CONCLUSIONS

Based on the RBSM, numerical model was developed to simulate the uni-axial tension behavior of reinforced concrete members strengthened with CFS. By adapting bond-slip models to simulate the concrete-steel/CFS interfaces, also bond deterioration models was developed to simulate the bond deterioration at the cracks locations. By comparing the numerical results with the experimental one, the following conclusions can be summarized;

1. The model can simulate the experimental observation in satisfied way.
2. CFS reduced the crack spacing so the average bond stress of the steel reinforcing bar became smaller.
3. The average bond stress of the CFS increased with number of layers of CFS.
4. The bond deterioration of concrete-steel/CFS interfaces due to cracking was simulated well by applying bond deterioration models.
5. The average yielding stress of the reinforcing bar increased with CFS ratio.

References

1) Kawai, T., New Element Models in Discrete Structural Analysis, J. of the Society of Naval Architects of Japan, No.141, pp.174-180, 1977.
2) Kawai, T., New Discrete Models and Their Application to Seismic Response Analysis of Structure, J., of Nuclear Engineering and Design, No. 48, pp. 207-229, 1987.
3) Bolander, J. E. and Saito, S., Fracture Analysis Using Spring Network Models with Random Geometry, J. of Engineering Fracture Mechanics, No. 61, PP. 569-591, 1998.
4) Japan Concrete Institute (JCI)., Technical Reports on Continuous Fiber Reinforced Concrete, TC952 on Continuous Fiber Reinforced Concrete, Tokyo, 1998.
5) Japan Society of Civil Engineers (JSCE), Guidelines for retrofitting of concrete structures-Draft, Concrete Library Int., 36, pp.61-112.
6) Sato, Y., Asano, Y., and Ueda, T., Fundamental study on bond mechanism of carbon fiber sheet. Concrete Library Int., 37, pp. 97-115.
7) Ueda, T., Yamaguchi, R., Shoji, K., Sato, Y., Study on behavior in tension of reinforced concrete members strengthened by carbon fiber sheet. Journal of Composite for Construction, ASCE, Vol. 6, NO. 3, pp. 168-174, 2002.
8) Hordijk, D., A., Local approach to fatigue of concrete, Thesis Technical University of Delft, pp. 66-77 , 1991
9) Saito, S., and Bolander, J. E., Numerical analysis of shrinkage cracking controlled by carbon fiber nets. Proceeding of 3rd International Symposium on Non-Metallic (FRP) reinforcement for Concrete Structures, Sapporo, Japan 2. pp. 275-282, 1997.
10) Shima, H. Chou, L. and Okamura, H., Micro and macro models for bond reinforced concrete., J. of the Faculty of Engineering, Tokyo University Vol.XXXIX, No. 2, PP. 133-194, 1987.
11) Goto, Y., Cracks formed in concrete around deformed tension bars, ACI Journal, Proceedings Vol. 68, No. 4, pp 244-251, 1971.
12) Qureshi, J. and Maekawa, K., Computational model for steel bar embedded in concrete under combined axial pullout and transverse shear displacement, Proc of JCI, Vol. 15, No., 2, pp. 1249-1254, 1993.
13) Okamura, H. and Maekawa, K.; Nonlinear Analysis And Constitutive Models of Reinforced Concrete, Gihodo, Tokyo, 1991.
14) Salem, H., and Maekawa, K.,: Spatially averaged tensile mechanics for cracked concrete and reinforcement under highly inelastic range., j. Materials, Conc. Struct. Pavements, JSCE, No., 613 Vol., 42, pp., 277-293, 1999.
15) Yamaguchi, R., A study on uni-axial tension behavior of RC members strengthened with carbon fiber sheet. Master dissertation. Hokkaido University, 2000